Flow enhancement in nanotubes of different materials and lengths

Konstantinos Ritos,[1,a)] Davide Mattia,[2] Francesco Calabrò,[3] and Jason M. Reese[4]
[1]*James Weir Fluids Lab, Department of Mechanical and Aerospace Engineering, University of Strathclyde, Glasgow G1 1XJ, United Kingdom*
[2]*Department of Chemical Engineering, University of Bath, Bath BA2 7AY, United Kingdom*
[3]*DIEI, Università di Cassino e del Lazio Meridionale, 03043 Cassino, Italy*
[4]*School of Engineering, University of Edinburgh, Edinburgh EH9 3JL, United Kingdom*

(Received 4 May 2013; accepted 27 November 2013; published online 2 January 2014)

The high water flow rates observed in carbon nanotubes (CNTs) have previously been attributed to the unfavorable energetic interaction between the liquid and the graphitic walls of the CNTs. This paper reports molecular dynamics simulations of water flow in carbon, boron nitride, and silicon carbide nanotubes that show the effect of the solid-liquid interactions on the fluid flow. Alongside an analytical model, these results show that the flow enhancement depends on the tube's geometric characteristics and the solid-liquid interactions. © *2014 AIP Publishing LLC*. [http://dx.doi.org/10.1063/1.4846300]

I. INTRODUCTION

In the last ten years, the enhancement of fluid flow in carbon nanotubes (CNTs) has been intensively investigated.[1] While there is now compelling evidence, from both experiments and molecular dynamics (MD) simulations, that liquid flow enhancement does indeed occur in nanotubes and other nanochannels, the origin of this phenomenon and how to control it is still subject to debate.[2] Some aspects are now generally accepted, including the nanotube diameter threshold below which the conventional continuum fluid mechanics model can no longer be applied,[3] the presence of a reduced viscosity or depletion layer near the tube wall due to solid-liquid molecular interactions,[4,5] that the flow enhancement is proportional to the tube length,[6] and that losses are mainly confined to the entrance region of the tube.[6–8]

Another important aspect is the nanotube wall structure and chemistry. While the effect of roughness on fluid flow is not clear, there is compelling evidence that modifying the surface chemistry can alter the flow velocity, and so the flow enhancement. MD simulations have shown that imposing hydrophilic potentials on a CNT structure would significantly reduce the flow enhancement.[4] A similar result can be obtained when introducing defects to the CNT structure.[9] Experiments have shown that functionalization of the entrance of CNT membranes can significantly alter capillary filling and flow enhancement,[10] and that surface modification of the CNTs can be used to control their ability to imbibe liquids of different nature.[11,12] MD simulations have also shown that functionalization of the CNT tips could be used to control selective permeation of ions through CNT membranes,[13] which is important for their potential use in water filtration and desalination applications.[14]

This latter aspect, in particular, has led to the development of models to understand the effect of the solid-liquid interactions on fluid flow in nanotubes. Initial developments focussed on relating the flow enhancement to the wetting behavior of the nanotubes, via the slip length.[15] Others have attributed the enhancement effect solely to a reduced fluid viscosity at the wall.[5,16] In contrast to this, a model based on the macroscopic Navier friction coefficient, calculated using a constant value of density and viscosity, has been recently proposed.[17–19] Each of these models is able to capture only some of the flow enhancement data in the literature, and they also make use of a number of fitting or semi-empirical parameters.

In this paper, we present new MD simulations of water flowing in CNTs, boron nitride nanotubes (BNNTs), and silicon carbide nanotubes (SiCNTs) in order to investigate the effect of the solid-liquid molecular interactions on the flow. The choice of these materials is motivated by the recent interest in constructing BNNT[20–22] and SiCNT[23,24] membranes, as first modeling results show that they could be strong competitors to CNT-based membranes in terms of permeability and selectivity.[25–34] Further, our MD results are analysed using a model recently developed by the authors[35] that makes explicit the dependence of the flow enhancement on both the tube geometry and the interactions between the nanotube wall and the flowing liquid. The combination of MD results and model sheds new light on the different physical effects that can help guide researchers in developing future nanotube membranes for specific applications.

II. SIMULATION METHODOLOGY

A. Molecular dynamics

We conduct molecular dynamics simulations of systems consisting of a membrane separating two water reservoirs that contain at least 25 000 water molecules. The pore of the membrane is a nanotube, which is made of either carbon, boron nitride, or silicon carbide. In order to separate the two reservoirs, and so form a membrane, two sheets made of the same material as the nanotube are placed at the entrance and exit of the nanotube (see Fig. 1). The investigated nanotubes have

a)Author to whom correspondence should be addressed. Electronic mail: konstantinos.ritos@strath.ac.uk

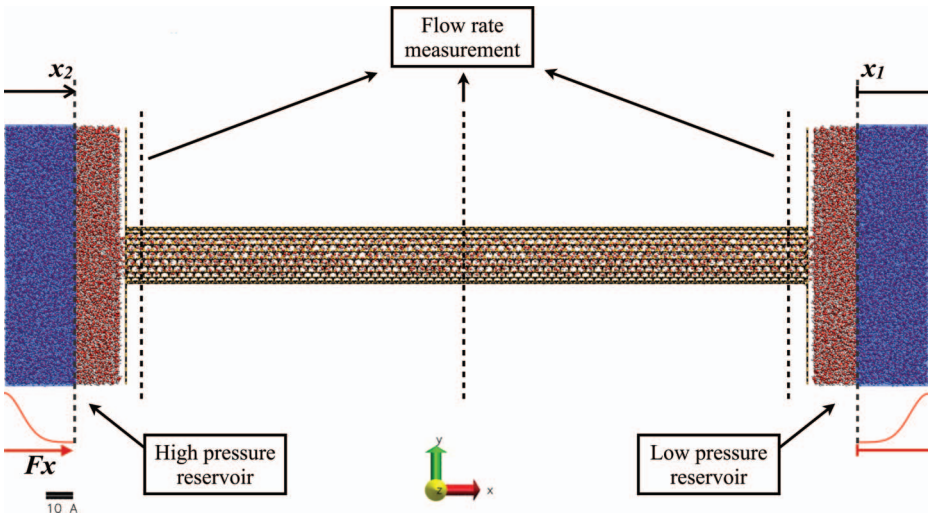

FIG. 1. The flow system for MD simulation: a nanotube connects two reservoirs, with water flowing along the nanotube from the high pressure side (left) to the low pressure side (right). Blue shaded areas are the MD control regions, where temperature and pressure are controlled. During equilibration runs, the density is also controlled in the same regions. In steady state conditions, flow rate measurements at the indicated measurement planes perfectly match each other.

a chirality of (15,15) in the case of CNTs and BNNTs, and (12,12) for SiCNTs. Taking into account the differences in bond lengths between these materials, the given chiralities correspond to a tube radius of 1.017 nm for the CNT, 1.036 nm for the BNNT, and 1.031 nm for the SiCNT. The thickness of the simulated membranes (i.e., the length of the nanotubes) is varied from 2.5 nm up to 50 nm. Periodic boundary conditions in all directions are applied, and the temperature in the reservoirs is controlled by Berendsen thermostats at a constant 298 K; in the longer (>25 nm) BNNTs and SiCNTs the z-component of the velocity is also thermalized along the nanotube in order to avoid excessive viscous heating. It takes around 7 days to simulate 1 ns of problem time on 24 CPU cores for nanotubes smaller than 12.5 nm, or 48 CPU cores for all other cases. The problem time for each of our MD simulations ranges from 10 ns to about 25 ns.

After an equilibration time of at least 5 ns, a pressure difference of 200 MPa between the two water reservoirs is imposed and then maintained constant. This high pressure difference enables steady state of the fluid flow to be reached in a reasonable time, thus reducing the computational cost of the simulations. It is common practice in MD studies, as no major spurious effects appear when compared to the low-pressure-difference case that is closest to actual operating conditions.[6,8,9,36–38] In addition, water thermal velocities are quite high, so a high flow velocity improves the signal-to-noise ratio in velocity profile measurements.

In previous publications, pressure difference control was achieved by imposing a uniform body force to all liquid molecules in the nanotube, for a standalone nanotube with periodic boundary conditions in the flow direction.[39–41] For more complex geometries, like the membranes in this paper, the overall cross-sectional area is not uniform (i.e., from reservoir to nanotube to reservoir), and so the pressure gradient will vary; fundamentally, a uniform body forcing is not capable of reproducing flows that are hydrodynamically equivalent to those generated by a pressure difference over the same geometry. Previous studies of similar systems have used moving walls, acting as pistons, in order to control the pressure difference between the reservoirs, although this option breaks the periodicity in the flow direction.[8,42]

In our simulations we instead impose a pressure difference between the two reservoirs by applying a Gaussian-distributed force over cross-sectionally uniform areas only (see the blue shaded regions in Fig. 1). This creates a known pressure drop over the entire system. This approach is a development of previous publications[36,43] in which step-forcing was used to create the necessary pressure difference. Our approach creates a spatially smooth imposition of momentum to the MD fluid, while maintaining the simplicity of using periodic boundary conditions. The magnitude of the imposed force in the shaded areas in Fig. 1 is

$$F_x(x) = \begin{cases} \bar{F} \exp\left\{-x^2/2\sigma_s^2\right\} & \text{if } x_1 \le x \le x_2 \\ 0 & \text{otherwise} \end{cases}, \qquad (1)$$

where σ_s is the standard deviation of the distribution and $\bar{F}$ is its peak value, i.e.,

$$\bar{F} = \frac{\Delta p}{\rho_n \sigma_s \sqrt{2\pi}}, \qquad (2)$$

with ρ_n the average number density inside the two reservoirs and Δp the desired pressure difference between them. The standard deviation σ_s can take any value provided that it is significantly smaller than the distance $x_2 - x_1$. A more detailed description of this Gaussian-forcing method is provided by Borg *et al.*[44]

In all the simulations presented here the rigid TIP4P/2005 water model is used,[45–47] which consists of a Lennard-Jones (LJ) 6-12 interaction potential at the oxygen atom site (O), positive coulomb charges at the two hydrogen sites (H), and a negative charge at a massless site (M), located a small distance away from O. The solid atoms of the membranes are kept fixed, which is a common simplification in MD simulations as it provides significant computational savings while generating only a small error in the measured flow

TABLE I. Lennard-Jones parameters between interacting atoms.

Interaction pair	σ (nm)	$\epsilon \times 10^{21}$ (J)
O–O	0.315890	1.286750
C–O	0.319000	0.709302
C_{SiC}–O	0.327776	0.705867
N–O	0.326169	1.135040
B–O	0.330352	0.919718
Si–O	0.329339	2.201310

rate.[3,4,48–50] The solid atoms interact with the water molecules through LJ and Coulomb potentials:

$$U_{6-12}(r_{ij}) = \begin{cases} 4\epsilon \left[\left(\frac{\sigma}{r_{ij}}\right)^{12} - \left(\frac{\sigma}{r_{ij}}\right)^{6} \right] & \text{if } r_{ij} < r_{cut} \\ 0 & \text{if } r_{ij} \geq r_{cut} \end{cases}, \quad (3)$$

$$U_{Coulomb}(r_{ij}) = \begin{cases} \frac{q_i q_j}{4\pi\epsilon_0} \left(\frac{1}{r_{ij}} - \frac{1}{r_{cut}} + \frac{1}{r_{cut}^2}(r_{ij} - r_{cut}) \right) & \text{if } r_{ij} < r_{cut} \\ 0 & \text{if } r_{ij} \geq r_{cut} \end{cases}, \quad (4)$$

where ϵ_0 is the vacuum permittivity 8.854×10^{-12} $C^2/(N\,m^2)$. Both type of interactions are truncated at a cutoff radius of $r_{cut} = 1.2$ nm (which is chosen according to previous publications[6,8,49] and after performing a sensitivity test), while Coulomb interactions are also shifted.[51] The LJ parameters of the water-carbon interactions for the CNT membranes (see Tables I and II) are chosen specifically for the TIP4P/2005 water model in order to reproduce the macroscopic contact angle of a water droplet on a graphitic surface, following the methodology of Werder *et al.*[49] Water molecules interact more strongly with BNNTs and SiCNTs, compared to CNTs, due to the electrostatic forces caused by the materials' polarity. For the much weaker van der Waals forces, represented here by Lennard-Jones interactions, the parameters used are from previously reported force fields and *ab initio* calculations for BNNTs[26] and SiCNTs[24,34] along with Kong's mixing rules.[52]

B. Measurement techniques

A series of flow property measurements are performed during each MD simulation at every timestep, and the reported results have always been time-averaged over at least 2.5×10^6 timesteps. Flux measurement planes are placed as shown in Fig. 1 to measure the net mass flow rate $\dot{m}$ (kg/s) along the nanotube. The mass of the total number of molecules that cross the target flux-plane in the x-direction is counted as positive, and the mass of those which cross in the opposite direction is counted as negative. The mass flow rate is then calculated by dividing the total mass flow counted by the time over which we perform the averaging,[6,44] i.e.,

$$\langle \dot{m} \rangle = \frac{1}{\Delta t_{av}} \sum_{i}^{\delta N} m_i \, \mathrm{sgn}\,(\boldsymbol{v}_i \cdot \hat{\boldsymbol{n}}_x), \quad (5)$$

where $\hat{\boldsymbol{n}}_x$ is the unit vector in the x-direction perpendicular to the flux-plane, $\boldsymbol{v}_i$ and m_i are the velocity vector and the mass of molecule i crossing the flux plane, and δN is the total number of molecules that cross the plane in either direction during the time $t \rightarrow t + \Delta t_{av}$. The function sgn () provides the crossing direction. The volumetric flow rate Q_{MD} is calculated by simply dividing $\langle \dot{m} \rangle$ by the water bulk density ρ. In order to compare the water flow performance of the various nanotube materials, the mass flow rate in every system was measured under the same conditions. After steady state conditions have been reached, measurements for a given nanotube at all three planes in Fig. 1 agree.

Radial density and velocity profile measurements provide further insight into the water structure inside the nanotubes and how the various tube materials affect the flow behavior. Each nanotube is divided into 100 radial cylindrical bins, and the density and the velocity are measured inside every bin over the full length of the nanotube, from the first flux measurement plane up to the third one. The results are averaged over a large number of MD timesteps.

Water axial self-diffusivity is also measured inside the nanotubes under equilibrium MD simulations, before any pressure difference is applied. Two equivalent methods to calculate the self diffusivity of a liquid or gas are often used,[53] the first one based on the time integration of the velocity autocorrelation function, and the second based on calculating the mean-squared displacement. In this paper the former was chosen, and D_s is calculated with the Green-Kubo expression,

$$D_s = \frac{1}{N} \int_0^\infty \sum_{i=1}^{N} \langle v_{i,x}(t) \cdot v_{i,x}(t + t') \rangle dt', \quad (6)$$

where $v_{i,x}\,(t)$ is the axial center of mass velocity of molecule i at some time t, and $\langle \cdots \rangle$ denotes the ensemble average. Equation (6) is an average over all N water molecules. The autocorrelation function decays quite quickly, and then fluctuates around zero, so a small time window of a few timesteps is enough to calculate D_s. A production simulation contains thousands of sampling time windows, and the reported values of D_s are averaged over all the collected samples. The same measurements are then repeated in steady flow conditions under an applied pressure difference, and show no significant difference. So pressure-driven flow inside nanotubes does not further alter water's self diffusivity[37] beyond that of the effect of confinement, as will be shown in Sec. III. From its self-diffusivity, the water viscosity μ can be calculated through the Stokes-Einstein relation,[5,31,54]

$$\mu = \frac{k_B T}{3\pi\alpha D_s}, \quad (7)$$

TABLE II. Charges on atoms of polar molecules.

Atom	$q\,(e)$
O	...
M	− 1.1128
H	0.5564
C	...
C_{SiC}	− 0.6000
N	− 1.0500
B	1.0500
Si	0.6000

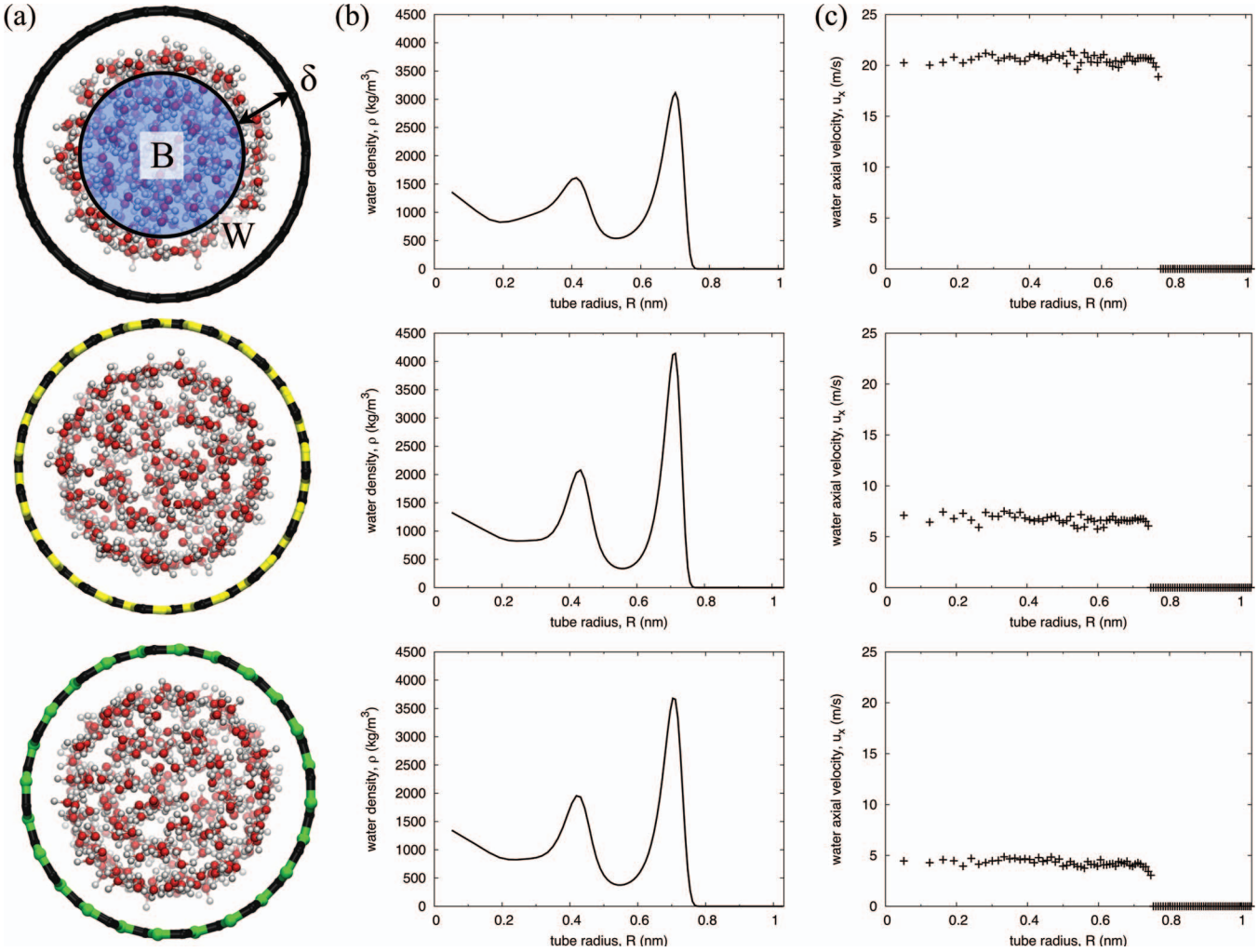

FIG. 2. (a) Cross-section snapshots of the three different nanotubes transporting water molecules. The nanotube material of the top snapshot is carbon, the middle is boron nitride, and the bottom is silicon carbide. The bulk region (B) is illustrated with light blue shading, and the annular region (W) (where the viscosity is reduced) has a thickness $\delta = 0.5$ nm, constant for all materials. (b) Water density profiles across the nanotube radii showing the concentric water ring structure. (c) Velocity profiles across the nanotubes for the same applied pressure difference of 200 MPa.

where k_B is Boltzmann's constant, T is the water temperature, and $\alpha = 1.7$ Å is the effective hydrodynamic diameter of a water molecule, which is calculated from the average positions of hydrogen atoms and charge sites relative to the oxygen atom in the TIP4P/2005 water model.[47,54]

Finally, the work of adhesion W_A, which is the potential energy from the interaction of the first water layer with the nanotube atoms divided by the nanotube surface area, is easily measured. The potential energy of every atom is readily available in MD simulations, as this is at the core of the MD algorithm. As a result, no special measurement technique is needed besides a summation of the potential energy of water molecules due to their interaction with the nanotube atoms in an annular region close to the nanotube wall.

III. RESULTS AND DISCUSSION

Figure 2(a) shows the structure of the water molecules inside carbon, boron nitride, and silicon carbide nanotube cross-sections, taken from characteristic simulations of membranes with 25 nm long nanotubes. In all cases, a highly ordered and packed layer of water molecules is formed close to the inner nanotube walls. This is more apparent from the radial density profiles in Fig. 2(b). This arrangement lends itself to the idea of modeling water inside the nanotubes as a two-fluid system, with a fluid viscosity in the annular region close to the wall that is distinct from the bulk fluid viscosity close to the tube's axis. The thickness of the annular region is very similar for all nanotube materials studied at $\delta = 0.5$ nm, which includes the "empty" region along with the first high-density water layer (Fig. 2), in agreement with previous MD work.[4,54] The averaged velocity profile across each nanotube is presented in Fig. 2(c). It is seen that water flows with minimum viscous losses and has a plug-like velocity profile for all three simulated materials. This is reflected in the variation of the flow rate with the pressure gradient for the three materials tested (Figure 3), with CNTs showing a significantly higher flow rate than BNNTs and SiCNTs. The deviations in this figure for the shortest tube lengths are attributed to a dominating effect of entrance losses in short tubes, as shown in the recent literature.[6–8]

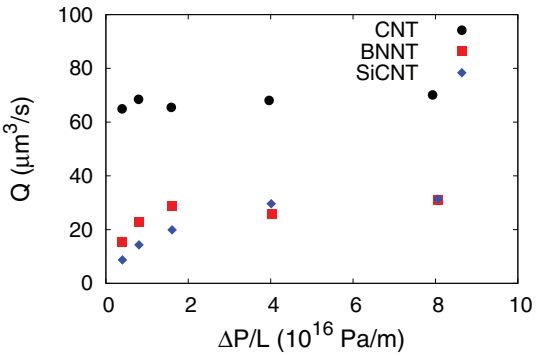

FIG. 3. Volumetric flow rate (Q) versus pressure gradient ($\Delta P/L$) for the three nanotube materials tested. CNTs show a 2- to 4-fold higher flow rate than BNNTs and SiCNTs, respectively, for the same pressure gradient. Standard deviation of all data points is smaller than 5%, with error-bars covered by the data-point symbols themselves. The standard error of the mean is smaller than 0.01% for all reported values.

To understand the difference in flow rates for the different nanotube materials, the MD results are analysed using a model recently developed by the authors[35] that makes explicit the relationship between flow enhancement (defined as the ratio of the measured MD flow rate to the conventional Hagen-Poiseuille prediction with no-slip boundary conditions, $\epsilon = Q_{measured}/Q_{HP}$) and the strength of the solid-liquid interactions occurring at the nanotube walls:

$$\epsilon = \left(\frac{R-\delta}{R}\right)^4 \left(1 - \frac{\mu_B}{\mu_W}\right) + \frac{\mu_B}{\mu_W}\left(1 + 8\mu_W \frac{L}{R^2}\frac{D_s}{W_A}\right), \tag{8}$$

where μ_B is the bulk viscosity of the fluid, μ_W is the viscosity of the fluid in the annular region near the tube wall (where the effect of the solid-liquid molecular interactions is the strongest), and D_s and W_A are the self-diffusivity of water molecules and the work of adhesion between the liquid and the channel wall, respectively. This model is based on the Hagen-Poiseuille equation but takes into account the molecular solid-liquid interactions at the wall, the tube geometrical characteristics, and water properties inside the nanotube. It has shown good agreement with previously reported experimental and computational results for carbon[35] and inorganic[55] nanotube materials. Details of the derivation of Eq. (8) can be found in Ref. 35. This equation contains no fitting parameters: as noted above, δ has been found to be the same for all three cases (Fig. 2), while D_s and W_A are constant values for any given solid-liquid couple and flow conditions. Both can be measured experimentally (for example, W_A can be measured via immersion calorimetry) or calculated via MD. The viscosities μ_B and μ_W are calculated from MD results using the Stokes-Einstein relation for water in the bulk and annular regions close to the wall, respectively, following an established MD methodology.[5,54] Table III reports the averaged values calculated from MD for each nanotube material. This table shows that the fluid viscosity close to the nanotube wall is always lower than the viscosity calculated in the center of the tube (the bulk flow). Furthermore, the bulk values differ from the value measured for the same water model in an unconfined environment,[46] so it can be deduced that confinement has a significant effect on the water viscosity.[5]

TABLE III. Average water properties calculated via MD for each nanotube material.

Material	$D_s \times 10^9$ (m^2/s)	$W_A \times 10^3$ (N/m)	$\mu_W \times 10^4$ (Pa s)	μ_W/μ_B
Carbon	3.14 ± 0.18	98.7 ± 0.42	7.02	0.29
Boron nitride	2.48 ± 0.10	184.0 ± 1.76	9.09	0.56
Silicon carbide	2.33 ± 0.06	164.5 ± 1.53	10.27	0.73

A measure of the reliability of calculating D_s and W_A through MD simulations can be obtained by comparing our MD results for CNTs in Table III with published data:[35] W_A for water on graphite (measured via immersion calorimetry) is 97×10^{-3} N/m; D_s for water on graphene and through graphitic slit pores has been found to be $(2\text{–}4) \times 10^{-9}$ m^2/s.[56] To the authors' knowledge, independent measures of these properties for boron nitride and silicon carbide are not yet available in the literature.

In Fig. 4 the flow enhancement data are plotted against the D_s/W_A ratio, which represents the strength of the solid-liquid interaction for each of the nanotube materials tested. A reasonable linear fit through all data points confirms what MD, experimental results, and Eq. (8) have previously suggested: the more hydrophobic the material comprising the nanotube walls, the higher the flow enhancement (for a polar liquid such as water).

In Fig. 5 the flow enhancement data for the three nanotube materials are re-plotted as a function of the tube aspect ratio (L/D) to highlight the linear dependence shown by both the MD results and the model. A deviation between the two for the shortest tubes is explained by the presence of significant entrance losses, as previously discussed. This same linear dependence has been observed in MD results for CNTs of comparable lengths.[6] Whether the dependence remains linear for much longer tubes is still a matter of debate: experimental results for very long tubes have shown proportionally high enhancement values (~60 000 for 125 μm CNTs[57] and ~400 000 for 4 mm long CNTs[58]). A recent publication, on the other hand, indicates that the linear dependence for tubes of comparable length to the ones analysed here is followed by a plateau in the flow enhancement for micrometer long CNTs. This is attributed to a combination of entrance/exit losses and

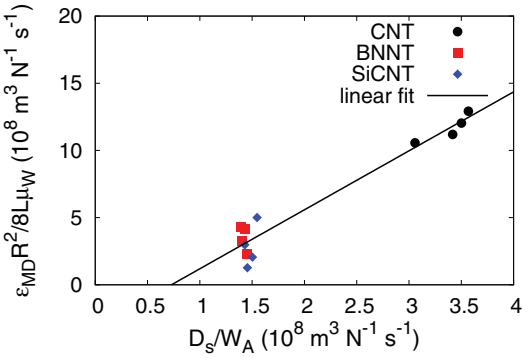

FIG. 4. Normalized flow enhancement as a function of the strength of solid-liquid interactions represented by the ratio D_s/W_A.

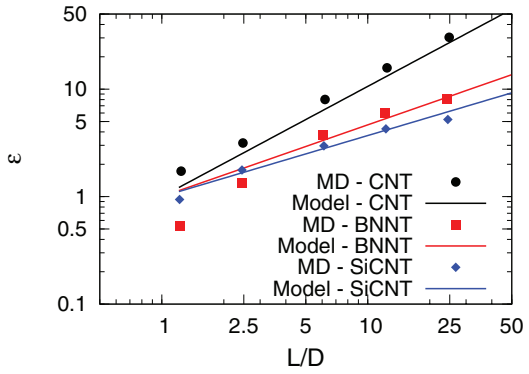

FIG. 5. Flow enhancement as a function of tube aspect ratio for CNTs, BNNTs, and SiCNTs of comparable diameter (∼2 nm). The model results for each material have been calculated using Eq. (8) and data from Table III. Standard deviation of all MD data points is smaller than 5%, with error-bars covered by data-point symbols themselves. The standard error of the mean is smaller than 0.01% for all reported values.

internal losses due to friction.[8] Addressing this issue requires further MD and experimental investigation, beyond the scope of this present work.

ACKNOWLEDGMENTS

The research leading to these results has received funding from the UK's Engineering and Physical Sciences Council (EPSRC) under Grant No. EP/I011927/1. D.M. and F.C. were funded by an International Joint Project of the UK's Royal Society. Results were obtained using the ARCHIE-WeSt High Performance Computer (www.archie-west.ac.uk), under EPSRC Grant No. EP/K000586/1. The authors thank the reviewers of this paper for their useful comments.

[1]M. Whitby and N. Quirke, Nat. Nanotechnol. **2**, 87 (2007).
[2]D. Mattia and Y. Gogotsi, Microfluid. Nanofluid. **5**, 289 (2008).
[3]J. A. Thomas and A. J. H. McGaughey, Phys. Rev. Lett. **102**, 184502 (2009).
[4]S. Joseph and N. R. Aluru, Nano Lett. **8**, 452 (2008).
[5]J. A. Thomas, A. J. H. McGaughey, and O. Kuter-Arnebeck, Int. J. Therm. Sci. **49**, 281 (2010).
[6]W. D. Nicholls, M. K. Borg, D. A. Lockerby, and J. M. Reese, Microfluid. Nanofluid. **12**, 257 (2012).
[7]T. Sisan and S. Lichter, Microfluid. Nanofluid. **11**, 787 (2011).
[8]J. H. Walther, K. Ritos, E. R. Cruz-Chu, C. M. Megaridis, and P. Koumoutsakos, Nano Lett. **13**, 1910 (2013).
[9]W. D. Nicholls, M. K. Borg, D. A. Lockerby, and J. M. Reese, Mol. Simul. **38**, 781 (2012).
[10]M. Majumder and B. Corry, Chem. Commun. **47**, 7683 (2011).
[11]D. Mattia, H. H. Bau, and Y. Gogotsi, Langmuir **22**, 1789 (2006).
[12]D. Mattia, M. P. Rossi, B. M. Kim, G. Korneva, H. H. Bau, and Y. Gogotsi, J. Phys. Chem. B **110**, 9850 (2006).
[13]B. Corry, Energy Environ. Sci. **4**, 751 (2011).
[14]K. P. Lee, T. C. Arnot, and D. Mattia, J. Membr. Sci. **370**, 1 (2011).
[15]C. Neto, D. R. Evans, E. Bonaccursi, H. J. Butt, and V. S. J. Craig, Rep. Prog. Phys. **68**, 2859 (2005).
[16]T. Myers, Microfluid. Nanofluid. **10**, 1141 (2010).
[17]J. S. Hansen, B. D. Todd, and P. J. Daivis, Phys. Rev. E **84**, 016313 (2011).
[18]K. Falk, F. Sedlmeier, L. Joly, R. R. Netz, and L. Bocquet, Langmuir **28**, 14261 (2012).
[19]S. K. Kannam, B. D. Todd, J. S. Hansen, and P. J. Daivis, J. Chem. Phys. **136**, 244704 (2012).
[20]M. Menon and D. Srivastava, Chem. Phys. Lett. **307**, 407 (1999).
[21]D. Golberg, Y. Bando, C. Tang, and C. Zhi, Adv. Mater. **19**, 2413 (2007).
[22]C. Zhi, Y. Bando, C. Tang, and D. Golberg, Mater. Sci. Eng. R **70**, 92 (2010).
[23]M. Menon, E. Richter, A. Mavrandonakis, G. Froudakis, and A. Andriotis, Phys. Rev. B **69**, 115322 (2004).
[24]K. Malek and M. Sahimi, J. Chem. Phys. **132**, 014310 (2010).
[25]C. Y. Won and N. R. Aluru, J. Am. Chem. Soc. **129**, 2748 (2007).
[26]C. Y. Won and N. R. Aluru, J. Phys. Chem. C **112**, 1812 (2008).
[27]M. E. Suk, A. V. Raghunathan, and N. R. Aluru, Appl. Phys. Lett. **92**, 133120 (2008).
[28]T. A. Hilder, D. Gordon, and S.-H. Chung, Small **5**, 2870 (2009).
[29]T. A. Hilder, D. Gordon, and S.-H. Chung, Small **5**, 2183 (2009).
[30]C. Y. Won and N. R. Aluru, Chem. Phys. Lett. **478**, 185 (2009).
[31]M. Khademi and M. Sahimi, J. Chem. Phys. **135**, 204509 (2011).
[32]R. Yang, T. A. Hilder, S.-H. Chung, and A. Rendell, J. Phys. Chem. C **115**, 17255 (2011).
[33]F. M. Garakani and R. Kalantarinejad, Int. J. Nano Dim. **2**, 151 (2012).
[34]T. A. Hilder, R. Yang, D. Gordon, A. P. Rendell, and S.-H. Chung, J. Phys. Chem. C **116**, 4465 (2012).
[35]D. Mattia and F. Calabrò, Microfluid. Nanofluid. **13**, 125 (2012).
[36]F. Zhu, E. Tajkhorshid, and K. Schulten, Biophys. J. **83**, 154 (2002).
[37]G. Raabe and R. J. Sadus, J. Chem. Phys. **137**, 104512 (2012).
[38]S. K. Kannam, B. D. Todd, J. S. Hansen, and P. J. Daivis, J. Chem. Phys. **138**, 094701 (2013).
[39]J. Koplik, J. R. Banavar, and J. F. Willemsen, Phys. Rev. Lett. **60**, 1282 (1988).
[40]K. P. Travis and K. E. Gubbins, J. Chem. Phys. **112**, 1984 (2000).
[41]X.-J. Fan, N. Phan-Thien, N. T. Yong, and X. Diao, Phys. Fluids **14**, 1146 (2002).
[42]L. Wang, R. S. Dumont, and J. M. Dickson, J. Chem. Phys. **138**, 124701 (2013).
[43]F. Zhu, E. Tajkhorshid, and K. Schulten, Biophys. J. **86**, 50 (2004).
[44]M. K. Borg, D. A. Lockerby, and J. M. Reese, Microfluid. Nanofluid. **15**, 541 (2013).
[45]J. L. F. Abascal and C. Vega, J. Chem. Phys. **123**, 234505 (2005).
[46]C. Vega and J. L. F. Abascal, Phys. Chem. Chem. Phys. **13**, 19663 (2011).
[47]D. J. Huggins, J. Chem. Phys. **136**, 064518 (2012).
[48]V. P. Sokhan, D. Nicholson, and N. Quirke, J. Chem. Phys. **117**, 8531 (2002).
[49]T. Werder, J. H. Walther, R. L. Jaffe, T. Halicioglu, and P. Koumoutsakos, J. Phys. Chem. B **107**, 1345 (2003).
[50]A. Alexiadis and S. Kassinos, Chem. Rev. **108**, 5014 (2008).
[51]J. S. Hansen, T. B. Schrøder, and J. C. Dyre, J. Phys. Chem. B **116**, 5738 (2012).
[52]L. A. J. Bastien, P. N. Price, and N. J. Brown, Int. J. Chem. Kinet. **42**, 713 (2010).
[53]D. Frenkel and B. Smit, *Understanding Molecular Simulation* (Academic Press, 2002).
[54]J. A. Thomas and A. J. H. McGaughey, Nano Lett. **8**, 2788 (2008).
[55]F. Calabrò, K. P. Lee, and D. Mattia, Appl. Math. Lett. **26**, 991 (2013).
[56]J. H. Park and N. R. Aluru, J. Phys. Chem. C **114**, 2595 (2010).
[57]M. Majumder, N. Chopra, R. Andrews, and B. J. Hinds, Nature **438**, 44 (2005).
[58]F. Du, L. Qu, Z. Xia, L. Feng, and L. Dai, Langmuir **27**, 8437 (2011).